Green's function method for the two-dimensional frustrated spin-$\frac{1}{2}$ Heisenberg magnetic lattice

Zhen Zhao,* Claudio Verdozzi,† and Ferdi Aryasetiawan‡
Division of Mathematical Physics and ETSF, Lund University, PO Box 118, 221 00 Lund, Sweden

(Received 12 July 2022; revised 3 November 2022; accepted 3 November 2022; published 21 November 2022)

The magnon Hedin's equations are derived via the Schwinger functional derivative technique, and the resulting self-consistent Green's function (GF) method is used to calculate ground state spin patterns and magnetic structure factors for two-dimensional magnetic systems with frustrated spin-$\frac{1}{2}$ Heisenberg exchange coupling. Compared with random phase approximation treatments, the inclusion of a self-energy correction improves the accuracy in the case of scalar product interactions, as shown by comparisons between our method and exact benchmarks in homogeneous and inhomogeneous finite systems. We also find that, for cross-product interactions (e.g., antisymmetric exchange), the method does not perform equally well, and an inclusion of higher corrections is in order. Aside from indications for future work, our results clearly indicate that the GF method in the form proposed here already shows potential advantages in the description of systems with a large number of atoms as well as long-range interactions.

DOI: 10.1103/PhysRevB.106.184417

I. INTRODUCTION

Due to the steady improvement of material fabrication procedures and high-resolution spin-resolved experimental techniques, in the past few decades, the list of magnetic phenomena and materials with complex magnetic order has grown at fast pace. Notable entries are, for example, magnetoresistance materials [1,2], helical magnets [3–6], and spin liquid systems [7,8], where interest from fundamental research in magnetic behavior merges with aims of technological exploitation in electronic devices.

An often distinctive trait of these systems is the occurrence of competing magnetic phases, which can change into each other upon a slight change of experimental conditions and sometimes even exhibit re-entrant behavior. This is, for example, what happens in $TlCuCl_3$ [9], where magnetic order can be tuned by applied pressure, or in the cubic chiral magnet $MnSi_{1-x}Ge_x$ [10], in which the spin texture is changed between skyrmion lattice and hedgehog lattice on Ge/Si substitution.

A key element in determining the variety of complex magnetic behaviors is magnetic frustration, which originates from different and competing magnetic couplings (e.g., spinel cubic materials, like $CoAl_2O_4$ [11,12] and $LiYbO_2$ [13]) or from specific spin lattice geometries, in which a given coupling cannot favor one among antagonistic magnetic configurations in a loop around a lattice plaquette [14] (as, e.g., for pyrochlore-lattice compounds [15]).

The notion of spin frustration is of quite general occurrence in magnetism [7,16–19]: indeed, it is highly relevant also for classical degrees of freedom (as, e.g., in Ising and Potts models) when, in the large-S limit, a classical treatment becomes appropriate. However, a quantum description is always in order for systems with spins $S < 1$, where strong quantum fluctuations are present. In this case, a customary way to describe frustration is via the quantum Heisenberg model (QHM), in which spins S localized at the nodes of a graph interact via (possibly long ranged) exchange interactions.

The QHM is a popular and flexible conceptual template that can include, among others, three-spin couplings [20], multipolar interactions [21], chiral spin-interactions [22], and quadratic anisotropy terms [23,24]. Importantly, the QHM is not only useful for its high pedagogical value: with a suitable choice of the model parameters (extracted, for example, by first-principles calculations [25–27]), it is often possible to obtain an accurate description of phase diagrams of real materials [24].

The QHM is also a paradigmatic test ground for theoretical methods, and extensive literature exists on the subject (see, e.g., Ref. [28]). However, despite a vast theoretical effort spanning almost a century, exact solutions are analytically known only in some specific cases: one-dimensional (1D) chains with only nearest-neighbor (NN) interactions [29], where the Bethe ansatz can be used; a square lattice with antiferromagnetic (AFM) NN interaction and diagonal dimerlike bond (the Shastry-Sutherland model) [30]; spin-$\frac{1}{2}$ systems on honeycomb lattices which can be reduced to free fermions within topological gauge theory (the Kitaev model) [31]. For more complicated flavors of the QHM, approximations become necessary (as, for example, in mean-field level approaches like spin-wave and bosonic methods [32]).

*Zhen.Zhao@teorfys.lu.se
†Claudio.Verdozzi@teorfys.lu.se
‡Ferdi.Aryasetiawan@teorfys.lu.se

Exact solutions to the QHM can also be obtained numerically, for example, via exact diagonalization (ED) [33,34] (applicable for any dimensionality but limited to very small samples), via quantum Monte Carlo (QMC) methods (based on stochastic algorithms) [28,35–38], and the density matrix renormalization group (DMRG) [39,40] (originally devised for 1D systems [39] but recently employed also for higher dimensions [41–44]). Fairly large samples can be treated within QMC and DMRG, which are useful to perform benchmark tests.

Both QMC and DMRG play a central role in our understanding of large but finite-sized clusters and periodic bulk systems with finite/short-range interactions; however, the case of long-range coupling, e.g., dipole interactions, is difficult to address with these approaches since the range of the interaction can be significantly longer than the size of cluster units computationally viable.

A way to overcome this issue is provided by the Green's function (GF) technique. Tyablikov [45] and Kondo and Yamaji [46] developed different decoupling methods within the random phase approximation (RPA) to solve the hierarchy problem in the equation of motion of GF. Similar decoupling methods have been used to study 1D and two-dimensional (2D) $S = \frac{1}{2}$ ferromagnets [47,48].

The GF technique can be applied with relatively low computational load to first-principles treatments of systems with effective spin-dependent interactions [49]. In addition, the Schwinger functional derivative technique for GF, which goes beyond the RPA decoupling, has been used to calculate the spin-wave spectra [50]. Furthermore, applications of the GF technique are not restricted to cluster models [51], which makes this technique a good candidate in the study of strongly coherent behavior and the magnetic structure factor of real materials and to address the case of long-range coupling.

II. PLAN OF THIS PAPER

Motivated by these considerations, in this paper, we introduce an approach to solve a finite $S = \frac{1}{2}$ 2D frustrated $J_1 - J_2$ QHM within the GF scheme. Our formulation is general and in principle exact, but as usual, an approximate scheme for vertex corrections beyond the RPA needs to be introduced. Since the magnetic structure factor is closely related to response functions, it is natural to adopt the Schwinger functional derivative technique when deriving the equations for the many-body correlation vertex, which then opens the way to systematically include corrections beyond the RPA.

The main outcomes of this paper are (i) derivation of the magnon Hedin's equations for the QHM, which are solved self-consistently within a scheme beyond the RPA; (ii) inclusion of impurities; (iii) calculations of the spin-correlation functions and the magnetic structure factor for a cluster system using the developed GF method; and (iv) comparisons against exact numerical benchmarks, which show that our approach provides fairly good accuracy with relatively low computational cost. Most importantly, and more in general, our results suggest that our method offers a practical, computationally advantageous route to investigate long-range interactions in the QHM.

The plan of the paper is as follows: in Sec. III, we introduce the system and the corresponding Hamiltonian and derive the magnon Hedin's equations via the Schwinger functional derivative technique in Sec. III A. In Sec. III B, we solve the equations in momentum space self-consistently for 2D lattices. Results and their discussion are presented in Sec. IV. Finally, in Sec. V, we provide some conclusive remarks and an outlook.

III. THEORY

The Schwinger functional derivative technique is used here to relate the high-order GF to the response of the lower-order one with respect to a probing field. The vertex equation of GF is derived and is solved self-consistently. The procedure presented here provides a formal justification of Tyablikov's [45] decoupling while at the same time producing improved results. We consider the isotropic QHM Hamiltonian:

$$H = -J_1 \sum_{<ij>} \hat{\mathbf{S}}_i \cdot \hat{\mathbf{S}}_j - J_2 \sum_{\ll ij \gg} \hat{\mathbf{S}}_i \cdot \hat{\mathbf{S}}_j - \sum_i \mathbf{B}_i \cdot \hat{\mathbf{S}}_i, \quad (1)$$

where $\hat{\mathbf{S}}_i$ is the (vector) spin operator associated with a 3-component spin at site i, $\mathbf{B}_i$ is the external magnetic field at site i, and $< ij >$ ($\ll ij \gg$) denote, respectively, NN and next NN (NNN) sites, with coupling constants J_1 (J_2).

The double-time GF is defined as

$$iG^{\alpha\delta}_{mn}(t_1, t_2) \equiv \left\langle T\left[\hat{S}^{\alpha}_m(t_1)\hat{S}^{\delta}_n(t_2)\right]\right\rangle, \quad (2)$$

where T is the usual time-ordering operator and $\langle \quad \rangle$ denotes a ground state average at zero temperature. The Greek letter superscripts refer to the spin components x, y, z, while mn are site indexes, and for the time variables, we henceforth use a simplified notation $t_i \to i$. With the spin ladder operators defined as $\hat{S}^{\pm} = \hat{S}^x \pm i\hat{S}^y$, the number of spin components can also be enlarged, i.e., $\alpha, \delta \in \{x, y, z\}$ or, equivalently, $\alpha, \delta \in \{+, -, z\}$. When $t_1 - t_2$ is an infinitesimal positive difference, GF provides the ground state correlation function, i.e.,

$$iG^{\alpha\delta}_{mn}(1^+, 1) = \left\langle \hat{S}^{\alpha}_m \hat{S}^{\delta}_n \right\rangle. \quad (3)$$

The property of the propagator from one space-time point to another is fully expressed with the components representing spin combinations $\{xx, xy, xz, \cdots, zz\}$, which can be written in matrix form or, equivalently, with the independent components $\{+-, zz\}$. For example, the equation of motion (eom) for G^{+-}_{mn} is

$$\begin{aligned} &i\partial_{t_1} G^{+-}_{mn}(1, 2) \\ &\quad = -2i \sum_{\tilde{i} \neq m} J_{m\tilde{i}} \left[G^{(3)z+-}_{m\tilde{i}n}(1, 1, 2) - G^{(3)z+-}_{\tilde{i}mn}(1, 1, 2) \right] \\ &\qquad + B^z_m(1) G^{+-}_{mn}(1, 2) + 2\delta(1-2)\delta_{mn}\langle \hat{S}^z_m(1) \rangle, \end{aligned} \quad (4)$$

where

$$G^{(3)\alpha\beta\delta}_{m\tilde{i}n}(1, 1, 2) \equiv \left\langle T\left[\hat{S}^{\alpha}_m(1)\hat{S}^{\beta}_{\tilde{i}}(1)\hat{S}^{\delta}_n(2)\right]\right\rangle \quad (5)$$

is a higher-order GF composed of three field operators, and $\tilde{i}$ labels the sites with nonzero exchange coupling to site m. For our system, $J_{m\tilde{i}} = J_1$ (J_2) when $\tilde{i}$ is the NN (NNN) site of m. Additional details can be found in the Supplemental Material (SM) [52].

Tyablikov's [45] method approximates the higher-order GF with

$$G^{(3)\alpha\beta\delta}_{\tilde{m}\tilde{i}}(1,1,2) \simeq \langle \hat{S}^{\alpha}_{m}\rangle\langle T\left[\hat{S}^{\beta}_{\tilde{i}}(1)\hat{S}^{\delta}_{n}(2)\right]\rangle + \langle \hat{S}^{\beta}_{\tilde{i}}\rangle\langle T\left[\hat{S}^{\alpha}_{m}(1)\hat{S}^{\delta}_{n}(2)\right]\rangle, \tag{6}$$

which works well with pure ferromagnetic (FM) or AFM systems. However, for frustrated systems, the simple factorization in Eq. (6) leads to discrepancies. In the following, the functional derivative method is used to derive the self-consistent equation for GF, giving a rigorous justification of Tyablikov's [45] approximation and extending the formulation to improve over it.

A. Schwinger derivative technique

In the interaction picture,

$$iG^{\alpha\delta}_{mn}(1,2) \equiv \frac{\langle\Psi|T\left[\hat{U}\hat{S}^{\alpha}_{m}(1)\hat{S}^{\delta}_{n}(2)\right]|\Psi\rangle}{\langle\Psi|\hat{U}|\Psi\rangle}, \tag{7}$$

where a local probing field **B** is contained in the evolution operator:

$$\hat{U} = T\exp\left[-i\int_{-\infty}^{\infty} d1\sum_{i}\hat{\mathbf{B}}_{i}(1)\cdot\mathbf{S}_{i}(1)\right]. \tag{8}$$

The higher-order GF can be related to the response of GF to the component of the local probing field:

$$i\frac{\delta G^{\alpha\delta}_{mn}(1,2)}{\delta B^{\beta}_{l}(3)} = iG^{(3)\beta\alpha\delta}_{lmn}(3,1,2) - G^{\alpha\delta}_{mn}(1,2)\langle\hat{S}^{\beta}_{l}(3)\rangle. \tag{9}$$

A self-energy can now be defined, making use of the eom and the functional derivative. Considering for concreteness the case $G_{mn} \equiv G^{+-}_{mn}$,

$$\sum_{i}\int d3\,\Sigma_{mi}(1,3)G_{in}(3,2) \equiv 2i\sum_{\tilde{i}} J_{m\tilde{i}}\left[\frac{\delta G_{mn}(1,2)}{\delta B^{z}_{\tilde{i}}(1)} - \frac{\delta G_{\tilde{i}n}(1,2)}{\delta B^{z}_{m}(1)}\right]. \tag{10}$$

A Hartree-like potential and an exchange-like potential can also be defined:

$$V^{H}_{m}(1) = \sum_{\tilde{i}} J_{\tilde{i}m}\langle\hat{S}^{z}_{m}(1)\rangle, \tag{11}$$

$$V^{F}_{m\tilde{i}}(1) = J_{\tilde{i}m}\langle\hat{S}^{z}_{m}(1)\rangle, \tag{12}$$

leading to a Dyson eom in terms of the self-energy:

$$\left[i\partial_{t_1} - V^{H}_{m}(1) - B^{z}_{m}(1)\right]G_{mn}(1,2) - \sum_{\tilde{i}\neq m} V^{F}_{m\tilde{i}}G_{\tilde{i}n}(1,2) - \sum_{i}\int d3\,\Sigma_{mi}(1,3)G_{in}(3,2) = 2\delta(1-2)\delta_{mn}\langle\hat{S}^{z}_{m}(1)\rangle. \tag{13}$$

Using the identity $\frac{\delta G}{\delta B}G^{-1} + G\frac{\delta G^{-1}}{\delta B} = 0$, the self-energy can be recast as

$$\Sigma_{mn}(1,2) = -i\sum_{\tilde{i}\neq m,l} J_{m\tilde{i}}\int d3\left\{G_{ml}(1,3)\frac{\delta G^{-1}_{ln}(3,2)}{\delta B^{z}_{\tilde{i}}(1)} - G_{\tilde{i}l}(1,3)\frac{\delta G^{-1}_{ln}(3,2)}{\delta B^{z}_{m}(1)}\right\}. \tag{14}$$

To solve for the response of G with respect to B, we take the functional derivative of Eq. (4) and neglect the second derivative term $\delta^2 G/\delta B^2$, thus obtaining

$$i\partial_1\frac{\delta G_{mn}(1,2)}{\delta B^{z}_{l}(3)} = G_{mn}(1,2)\delta(1-3)\delta_{ml} + \sum_{\tilde{i}\neq m} J_{m\tilde{i}}\left\{\frac{\delta\langle\hat{S}^{z}_{\tilde{i}}(1)\rangle}{\delta B^{z}_{l}(3)}G_{mn}(1,2) + \langle\hat{S}^{z}_{\tilde{i}}(1)\rangle\frac{\delta G_{mn}(1,2)}{\delta B^{z}_{l}(2)} - \frac{\delta\langle\hat{S}^{z}_{m}(1)\rangle}{\delta B^{z}_{l}(3)}G_{\tilde{i}n}(1,2) - \langle\hat{S}^{z}_{m}(1)\rangle\frac{\delta G_{\tilde{i}n}(1,2)}{\delta B^{z}_{l}(2)}\right\} + 2\frac{\delta\langle\hat{S}^{z}_{m}(1)\rangle}{\delta B^{z}_{l}(3)}\delta_{mn}\delta(1-2). \tag{15}$$

To solve for the response function $R_{ml}(1,2) = \frac{\delta\langle S^{z}_{m}(1)\rangle}{\delta B^{z}_{l}(2)}$, we look at the eom for $\langle\hat{S}^{z}_{m}(1)\rangle$:

$$\partial_1\frac{\delta\langle\hat{S}^{z}_{m}(1)\rangle}{\delta B^{z}_{l}(2)} = i\sum_{\tilde{i}\neq m} J_{m\tilde{i}}\frac{\delta}{\delta B^{z}_{l}(2)}\langle\hat{S}^{+}_{i}(1)\hat{S}^{-}_{m}(1)\rangle = \sum_{\tilde{i}\neq m,pq} J_{m\tilde{i}}\int d3d4G_{\tilde{i}p}(1^{+},3)\frac{\delta G^{-1}_{pq}(3,4)}{\delta B^{z}_{l}(2)}G_{qm}(4,1). \tag{16}$$

Starting with G computed at the mean-field level, the set of Eqs. (11)–(16) can be solved self-consistently. Then using Eq. (3), the observables as ground state expectation values and correlation functions can be computed from the equal-time GF. More details about the derivative technique can be found in the SM [52].

B. Solving the equations in momentum space

The magnon Hedin's equations in the last section were expressed in real space. Considering the time translational and spatial symmetries of the system, a Fourier transform provides GF in momentum-frequency space:

$$G_{mn}(1,2) \equiv G_{mn}(t_1,t_2) = \int d\omega\int d\mathbf{k}G(\mathbf{k},\omega)\exp[i\mathbf{k}\cdot(\mathbf{r}_m - \mathbf{r}_n)]\exp[-i\omega(t_1-t_2)]. \tag{17}$$

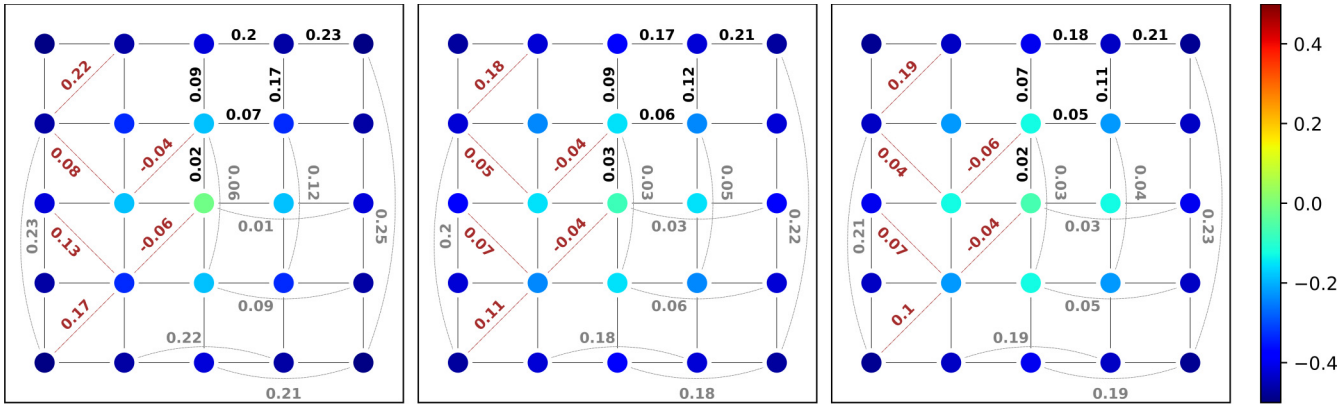

FIG. 1. Comparison between random phase approximation (RPA; left panel), exact diagonalization (ED; middle panel), and Green's function (GF; right panel) results for a 5×5 lattice with open boundary conditions. The results are for the $S^z_{\text{total}} = \frac{17}{2}$ subspace, with ferromagnetic (FM) exchange parameters: $J_1 = 1, J_2 = -0.5$. The color coding in the vertical bar applies to all panels.

The vertex function is now defined as

$$\Lambda_{p,q,l}(1,2,3) \equiv \frac{\delta G^{-1}_{pq}(1,2)}{\delta B^z_l(3)}, \tag{18}$$

which can be written in momentum-frequency space accordingly:

$$\begin{aligned}\Lambda_{p,q,l}(1,2,3) &\equiv \Lambda_{p,q,l}(t_1,t_2,t_3)\\ &= \int d\mathbf{k}d\mathbf{k}'d\omega d\omega' \exp[i\mathbf{k}\cdot(\mathbf{r}_p-\mathbf{r}_q)]\exp[i\mathbf{k}'\cdot(\mathbf{r}_p-\mathbf{r}_l)]\exp[-i\omega(t_1-t_2)]\exp[-i\omega'(t_1-t_3)]\Lambda(\mathbf{k},\mathbf{k}';\omega,\omega').\end{aligned} \tag{19}$$

In the $(\mathbf{k},\omega)$ space, our equations read

$$[\omega - V^{\text{HF}} - B^z]G(\mathbf{k},\omega) = \Sigma(\mathbf{k},\omega)G(\mathbf{k},\omega) + \langle S^z\rangle, \tag{20}$$

$$\omega R(\mathbf{k},\omega) = J(\mathbf{k})\int d\mathbf{k}'d\omega' G(\mathbf{k}+\mathbf{k}';\omega+\omega')\Lambda(\mathbf{k},\mathbf{k}';\omega,\omega')G(\mathbf{k}',\omega'). \tag{21}$$

Here, $V^{\text{HF}} = V^{\text{H}} + V^{\text{F}}$, and $V^{\text{H}}, V^{\text{F}}$, and $\langle S^z\rangle$ are the Fourier transforms of their corresponding real space-time values.

IV. RESULTS AND DISCUSSIONS

In this section, the approach introduced in Sec. III is applied to 2D Heisenberg systems with square and hexagonal lattices and different types of exchange coupling. To assess the performance of the method, the GF results are compared with numerical benchmarks from the ED method.

A. The case of a 2D square-lattice cluster

The system we consider is a 5×5 lattice with open boundary conditions. We discuss both FM and AFM magnetic regimes in a few selected subspaces with total spin projection S^z_{total}. Compared with either the FM limit $(25\uparrow, 0\downarrow)$ or the AFM one $(13\uparrow, 12\downarrow)$, an intermediate value of S^z_{total} shows most clearly the competition of NN and NNN exchange couplings. Thus, it is convenient to start the discussion with the subspace $S^z_{\text{total}} = \frac{17}{2}$ $(21\uparrow, 4\downarrow)$. We use the parameters $J_1 = 1, J_2 = -0.5$. The results are shown in Fig. 1, where we compare RPA, ED, and GF results. The color palette is used to represent the expectation value of the z-component spin $\langle S^z_m\rangle$, and the numbers show the z-z spin correlation between lattice points $\langle S^z_m S^z_n\rangle$.

Compared with the RPA decoupling method, the inclusion of the self-energy in the GF method gives higher accuracy for both $\langle S^z_m\rangle$ and $\langle S^z_m S^z_{\bar{m}}\rangle$, as shown by the improved locations of the poles of GF. The reason behind the improvement is that the direct response $\delta G/\delta B$, which is either treated as a constant (possibly with value 0) in the RPA method, gives a nonzero dynamical contribution to the self-energy. Therefore, the approximation used in the derivation of self-consistent equations in Sec. III A is the key step forward compared with the bare decoupling. Including higher-order responses $\delta^n G/\delta B^n$ can in principle improve the accuracy but at the cost of increased converging difficulties and heavier computational burden.

Our self-energy GF shows good accuracy also for $J_1 = -1, J_2 = 0.5$, $S^z_{\text{total}} = \frac{17}{2}$. Such parameters lead to pure AFM interaction (i.e., no frustration) on the square lattice. In the $S^z_{\text{total}} = \frac{17}{2}$ subspace, where most of the configurations are spin up, the ground state due to the AFM couplings is relatively homogeneous. This is detailed in Fig. 2, where $-0.45 \leqslant \langle S^z_m\rangle \leqslant -0.27$ and $\langle S^z_m S^z_n\rangle > 0$ for all lattice sites.

With the same couplings but for the $S^z_{\text{total}} = \frac{1}{2}$ subspace, the GF method describes well the Néel-type ground state: the

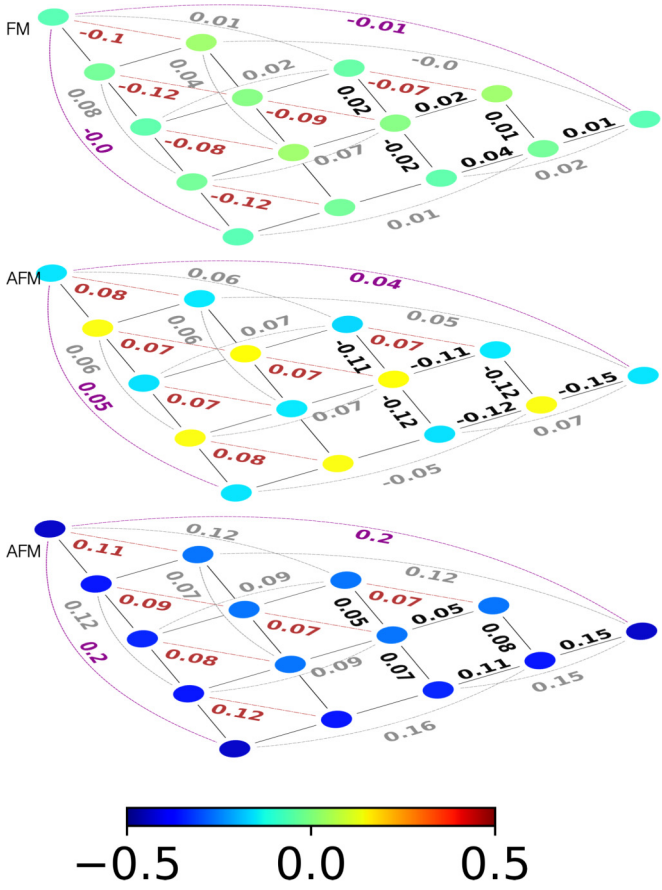

FIG. 2. $\langle S_m^z \rangle$ (denoted by color) and $\langle S_m^z S_n^z \rangle$ (denoted by numbers) for a 5×5 square lattice system with open boundary conditions. The color coding in the vertical bar applies to all cases, and results in each panel fulfill the C_{4v} square symmetry. Bottom panel: antiferromagnetic (AFM), $S^z_{\text{total}} = \frac{17}{2}$. Middle panel: AFM, $S^z_{\text{total}} = \frac{1}{2}$. Top panel: ferromagnetic (FM), $S^z_{\text{total}} = \frac{1}{2}$. The AFM coupling parameters are $J_1 = -1, J_2 = 0.5$, and the FM ones are $J_1 = 1, J_2 = -0.5$.

distribution of $\langle S_m^z \rangle$ is bipartite; sites on the same/different sublattices are positively/negatively correlated.

Remaining in the $S^z_{\text{total}} = \frac{1}{2}$ subspace but this time with $J_1 = 1, J_2 = -0.5$, we observe that the GF ground state has a small total spin value: the magnitudes of $\langle S_m^z \rangle$ are close to zero; NN sites are weakly correlated compared with $S^z_{\text{total}} = \frac{1}{2}, J_1 = -1, J_2 = 0.5$. This behavior is reminiscent of what occurs for systems with an even number of sites, where Lieb's theorem states that $S_{\text{total}} = 0$ in the ground state. For the three scenarios discussed above, the ground states are either relatively homogeneous (the signs of the exchange couplings and the net value of S^z_{total} in the given subspace are chosen so that they impose conflicting constraints on the spin alignment) or bipartite. This suggests that, for these cases, quantum fluctuations introduced by higher-order response terms play only a small role in the determination of GF.

Additional perspective on the method performance can be gained from the static spin structure factor, defined as

$$S(\mathbf{q}) = \frac{1}{N^2} \sum_{mn} \langle S_m^z S_n^z \rangle \exp[i\mathbf{q} \cdot (\mathbf{R}_m - \mathbf{R}_n)], \tag{22}$$

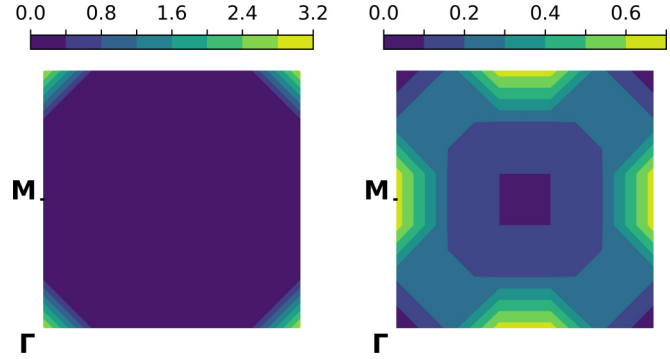

FIG. 3. Static structure factor $S(\mathbf{q})$ ($\mathbf{q} \in [0, 2\pi] \times [0, 2\pi]$) of a 5×5 square lattice with periodic boundary conditions and $J_1 = 1$, $J_2 = -0.5$. Left: $S^z_{\text{total}} = \frac{17}{2}$. Right: $S^z_{\text{total}} = \frac{1}{2}$. The high-symmetry points in the first Brillouin zone are labeled by $\mathbf{\Gamma} \equiv (0, 0)$ and $\mathbf{M} \equiv (0, \pi), (\pi, 0)$.

for a 5×5 lattice with periodic boundary condition. Because we are considering a square (i.e., bipartite) lattice, a Néel-like order is not compatible with a cluster with an odd number of atoms and periodic boundary conditions. Thus, we consider a 5×5 (4×4) cluster for FM (AFM) NN exchange. The GF results for $S(\mathbf{q})$ for a 5×5 FM cluster are shown in Fig. 3. The structure factor is strongly peaked at the $\mathbf{\Gamma}$ point for $S^z_{\text{total}} = \frac{17}{2}$ and relatively weakly peaked at $\mathbf{M}$ points for $S^z_{\text{total}} = \frac{1}{2}$, which agrees with previous results in the literature [53].

The displayed GF results are in very good agreement with the ED ones, and the differences between the two treatments are indistinguishable on the scale of the figure. Similar considerations apply to the agreement between GF and ED methods for a 4×4 cluster (not shown). We conclude this section by noting that the GF method in the frequency domain can also give direct access to the dynamical structure factor $S(q, \omega)$. However, to benchmark the GF-based $S(q, \omega)$ against exact ED results for the cluster sizes as discussed here, it may be necessary to employ the full ED Krylov subspace recursive techniques (beyond ground state ED). Computational development in this direction is under way.

B. Single- and double-impurity configurations

In realistic cases, one is often faced with the problem of having impurities in the system under investigation. Impurity atoms can be included by introducing an additional term in the Hamiltonian:

$$H_{\text{imp}} = -\sum_{ij} \Delta J_{ij} \hat{\mathbf{S}}_i \cdot \hat{\mathbf{S}}_j. \tag{23}$$

where either i or j denotes the impurity site(s). In the following, we specialize to the cases of single and double impurities in a 19-site hexagonal lattice and choose to work in the subspace $S^z_{\text{total}} = \frac{9}{2}$ which, as for the square lattice, nicely illustrate the interplay of FM and AFM couplings. In the no-impurity case, the coupling parameters are $J_1 = 1, J_2 = -0.5$; in the presence of impurities, we have the additional coupling strengths $\Delta J_{ij,\text{NN}} = 0.5 J_1$, $\Delta J_{ij,\text{NNN}} = 0.5 J_2$. The GF result is shown in Fig. 4. It is convenient for the discussion to organize the lattice sites in shells, where sites in a given shell

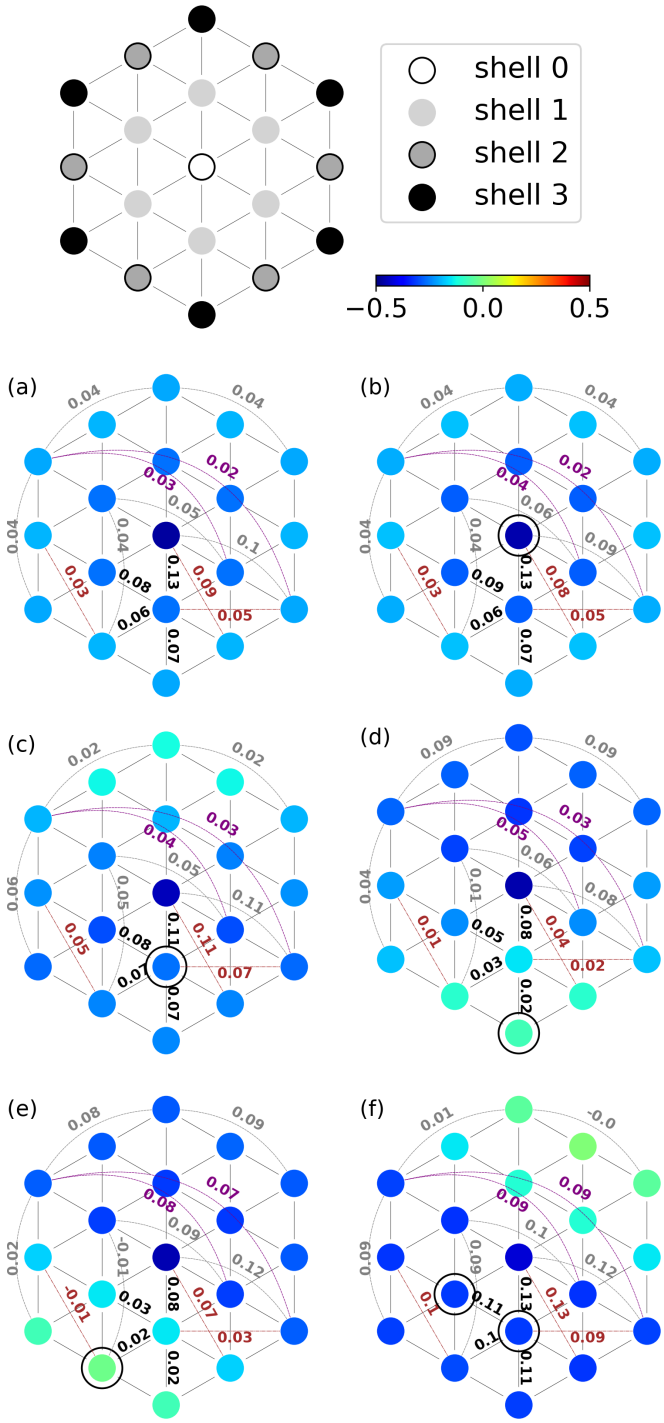

FIG. 4. $\langle S_m^z \rangle$ (denoted by color) and $\langle S_m^z S_n^z \rangle$ (denoted by numbers) in an open-boundary 19-site hexagonal lattice system with and without impurity. The nonimpurity coupling parameters are $J_1 = 1, J_2 = -0.5$. The additional impurity coupling strengths are $\Delta J_{\rm NN} = 0.5 J_1$, $\Delta J_{\rm NNN} = 0.5 J_2$. $S^z_{\rm total} = \frac{9}{2}$ ($14 \uparrow 5 \downarrow$). The top panel illustrates different shells of atoms (see main text). The color coding in the horizontal bar applies to all cases. (a) No impurity case. (b)–(f) The circles with a black outline are impurity sites.

are equally distant from the central site, and different shells correspond to different distances (Fig. 4).

For the nonimpurity case [Fig. 4(a)] and because of the FM NN couplings and the C_{6v} lattice symmetry, the central spin assumes the spin-down $\downarrow$ configuration. With $\langle S_m^z \rangle < 0$ and $\langle S_m^z S_n^z \rangle > 0$ at all sites, we then conclude that the nonimpurity system is dominated by FM interactions.

Inserting one impurity in the system amplifies both NN and NNN couplings. Locating the impurity at the center [Fig. 4(b)] effectively increases the FM strength around the impurity, which can be seen from the increased correlation between the impurity site and its NN. When the impurity moves away from the cluster center, the C_{6v} symmetry is broken. If the impurity is in shell 1 [Fig. 4(c)], the number of its FM NN sites remains 6, while the number of its AFM NNN sites decreases. Accordingly, the couplings between the impurity and its NN are FM dominated, and thus, the spins maintain the $\downarrow$ configuration. However, when the impurity atom moves to the boundary of the lattice [Figs. 4(d) and 4(e)], the value of spin-z projection at the impurity $\langle S_I^z \rangle$ is close to zero. This change of $\langle S_I^z \rangle$ when moving from the center toward the cluster boundary (where the number of NN and NNN sites is smaller) can be ascribed to the change in the number of neighbors, i.e., the finite-sized effect and the geometry of the cluster play important roles. Finally, we also show results for one geometry with two impurities, where the latter are both located in shell 1 and NN to each other [Fig. 4(f)]. In this case, the impurities and their NN spins are strongly FM coupled and form a small FM subcluster.

The results presented in Fig. 4, which were obtained with our GF technique, compare very well with ED calculations (not shown, differences of $\langle S_m^z \rangle$ between ED and GF are indistinguishable on the color scale of the figure). Furthermore, the trends for other $S^z_{\rm total}$ subspaces are very similar, with the same level of agreement between GF and ED schemes.

As an overall remark to this section, the GF approach appears to be able to capture all the effects due to the $J_1 - J_2$ competition, also in the presence of significant finite-sized effects. However, it should also be noted that the type of spin-spin interactions considered in this paper so far are symmetric in nature (i.e., expressed in terms of scalar products between spins). In many materials, the spin-orbit interaction can mediate antisymmetric exchange couplings among spins. This more challenging situation is addressed in the next section.

C. Including Dzyaloshinskii-Moriya interactions

The Dzyaloshinskii-Moriya interaction (DMI), also referred to as antisymmetric exchange [54,55], results from the interplay of spin-orbit and super-exchange interactions. The DMI can be written as

$$H_{\rm DM} = D \sum_{<ij>} \mathbf{e}_{ij} \cdot (\hat{\mathbf{S}}_i \times \hat{\mathbf{S}}_j), \tag{24}$$

where $\mathbf{e}_{ij} = (\mathbf{r}_j - \mathbf{r}_i)/|\mathbf{r}_j - \mathbf{r}_i|$ is the unit vector pointing from site i to site j. The DMI favors chiral canting of the spins and is thus responsible for the emergence of complex spin patterns, for example, magnetic skyrmions. Here, we wish to see how the GF method performs when DMI is present. To this end, we consider a system described by the Hamiltonian of Eq. (1) to which the term $H_{\rm DM}$ of Eq. (24) is added. In the presence of DMI, a diagonalization partitioned in subspaces with definite $S^z_{\rm total}$ is not possible, and thus, we consider a rather small (3×3) isolated cluster subject to an external field

TABLE I. Comparison between ED and GF on a 3×3 cluster. a refers to the bottom-left site, b refers to the left-middle site, and c refers to the center site. The lattice symmetry requires that $\langle S_c^x \rangle = \langle S_c^y \rangle = 0$, so neither of them is listed in the table.

	$\langle S_a^x \rangle$	$\langle S_a^y \rangle$	$\langle S_a^z \rangle$	$\langle S_b^x \rangle$	$\langle S_b^y \rangle$	$\langle S_b^z \rangle$	$\langle S_c^z \rangle$
ED	0.05	−0.05	0	0	−0.13	0.05	0.27
GF	0.12	−0.12	0.04	0	−0.23	0.14	0.34

$(0, 0, B)$, with FM parameters $J_1 = 1, J_2 = 0, B = 0.1$. The value chosen for the DMI is $D = 4$, which for the cluster considered provides noticeable canting of the spins. On inclusion of the DMI, there is a significant discrepancy between GF and ED spin patterns (as is shown in Table I, our GF approach fails to capture that the spins on the corner site of the cluster are completely in plane), indicating that, at least for this small system, a large vertex correction beyond the RPA is needed (this cannot be easily provided by a low-order self-energy as the one considered in Sec. III). To investigate the source of such a discrepancy, we consider the imaginary part of G_{12}^{+-}. In Fig. 5, we show the results for $\mathrm{Im}\, G_{12}^{+-}$, obtained both via our self-energy treatment and by applying spin operators on the ED ground state.

The GF and ED curves show similar generic trends, but for more detailed features, the two treatments are clearly at variance, with some specific structures differing both in position and strength. The locations of poles of ImG from ED are overall more compactly distributed, especially at positive frequencies. This discrepancy, also observed for other GF components (and for the real part of the GF as well) when DMI is present, is likely to be a general shortcoming of the GF approach within the linear response approximation and indicates the need to include the nonlinear response. The quality of the GF solution in the presence of DMI is considerably better when we place the 3×3 quantum spin cluster as the center block of a 9×9 lattice, and the remaining lattice points are occupied by mutually interacting classical spins with magnitude $|\vec{S}| = \frac{1}{2}$ that also interact with the quantum spins. Mixed quantum-classical systems can be useful to gain insight in large systems when the spin pattern develops over several lattice distances, and a quantum treatment of all spins

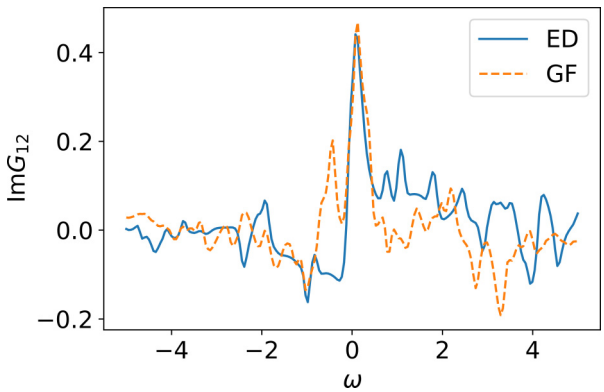

FIG. 5. Imaginary part of the G_{12}^{+-} component of the Green's function in the frequency domain.

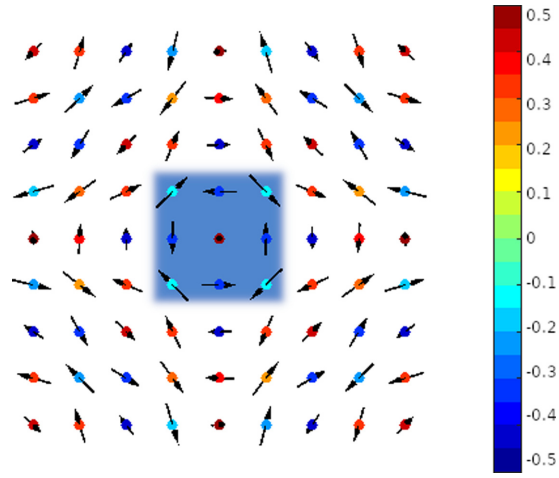

FIG. 6. Quantum spins (shaded region) in the background of classical spins. The arrow represents the spin projection in the xy plane, the color represents the S^z for classical spins and $\langle S^z \rangle$ for quantum spins. The coupling parameters are the same as in the 3×3 pure quantum case.

is computationally not viable (as, for example, in the case of magnetic skyrmions [56]). For our 9×9 system, we use a mixed quantum-classical self-consistent description where the quantum spins on the cluster border interact with the neighboring classical spins according to $-\sum_{qc} J_{qc} \hat{S}_q \cdot \vec{S}_c$. For a suitable choice of the J_1, J_2, D, and B parameters, a skyrmion-like ground state is expected to occur in the system. Here, we do not perform an extensive parameter search to establish the skyrmion regime. Rather, and for sake of comparison, the coupling parameters used are the same as in the isolated 3×3 quantum-spin cluster, and the results thus obtained are shown in Fig. 6. Within the figure resolution, the results from the self-energy approach and ED are not distinguishable. Furthermore, they differ from those of the isolated cluster. From the figure, no skyrmion-like pattern is easily discernible; however, an interesting qualitative aspect is that the ED and GF solutions compare well, due to the action of the forcing field due to the classical spins.

Naturally, there is at this point no way to say for certain if the similar ED and GF solutions describe well the full quantum exact solution for the 9×9 cluster. However, as an overall and final remark to the results of this section, we note that, unlike the Heisenberg exchange coupling, the DMI involves the cross-product of the spin operators. Such a difference in structure and symmetry of the Hamiltonian leads to a very different structure of the magnon Hedin's equations. In the derivation in Sec. III A, the higher-order response of GF is approximated with zero. The approach shows a good result for scalar-product exchange couplings but probably requires more considerations for interactions involving cross-product couplings.

V. CONCLUSIONS AND OUTLOOK

Remarkable progress has been made in understanding magnetism in condensed matter from a microscopic perspective. However, as of today, describing complex magnetic

configurations in real materials largely remains an open problem. This is because long-ranged magnetic patterns emerge from a delicate balance of several factors: among the most important are electronic correlations, electron-phonon interactions, crystal field effects, spin-orbit interactions, disorder, and impurities. Additionally, the number of atoms involved in the periodic unit (for commensurate order) of such magnetic textures can often be quite large (and unlimited for incommensurate order) which currently makes accurate first-principles descriptions challenging if not prohibitive.

An often adopted strategy is to turn to spin model Hamiltonians, with parameters extracted for first-principles calculations. This considerably simplifies the problem but without necessarily making it easily solvable. A case in point is provided by the QHM, the model in focus in this paper: Exact numerical methods like ED, DMRG, or Monte Carlo can be applied for not too large samples, and highly valuable information can be extracted for FM, AFM, and ferrimagnetic orders.

However, for many atoms/spins in the magnetic pattern, a significant increase in size is needed, (as, e.g., for dipolar interactions or when antisymmetric exchange couplings are present); here, using spatial/spin symmetries, the computational difficulty can be mildly reduced but not eliminated. As a concrete example, for magnetic skyrmions, it is the antisymmetric exchange that leads to the specific spin texture. For this type of exchange coupling, the total spin-z operator does not commute with the Hamiltonian, and configurations with different spin-z are mixed. Furthermore, skyrmion spin textures extend over several lattice distances, and direct exact numerical methods become inadequate at these sizes.

The alternative considered in this paper is the GF formalism that, even for considerable lattice/cluster sizes, remains quite affordable from the computational point of view. In this paper, we have derived the magnon Hedin's equations via the Schwinger functional derivative technique and applied the GF method to solve the Heisenberg model on 2D lattices, comparing the results with ED benchmarks. Our approach works well within the linear response regime. Higher-order approximations could also be considered, but this will increase the computational time and introduce additional hurdles in the convergence to self-consistency.

Concerning the numerical results, on the one hand, for a $J_1 - J_2$ model on square and hexagonal lattices, the GF scheme beyond the RPA gives reasonable accuracy with relatively low computational costs (in our comparisons, the limiting factor for the size of the clusters was in fact the ED treatment). The considerations apply to both ground state spin patterns and to magnetic structure factor results. Furthermore, the same level of agreement was found for inhomogeneous clusters in the few-impurity limit.

On the other hand, a preliminary attempt to apply the GF scheme to systems with an antisymmetric exchange interaction was not equally satisfactory. Our results suggest that a cross-product spin coupling may require a better approximate prescription than the neglect of the high-order response of GF to the probing field. Possible procedures for improvements in this direction are currently being explored.

Finally, based on the outcomes of this paper, we expect that the current approach (and the inherent approximation scheme used here) will work for long-range scalar product (e.g., magnetic-dipole) interactions. Preliminary tests also show that several hundreds of sites/spins are within reach of the method, and thus, we expect that the method could be successfully employed for systems of higher dimensionality. As another follow up of this paper, we plan to investigate systems with magnetic dipole interactions and compare the GF results with experimental values. Quite naturally, the long-term goal is to improve the GF scheme in a way that it would become possible to accurately calculate the magnetic structure factor of real materials.

ACKNOWLEDGMENTS

F.A. gratefully acknowledges financial support from the Knut and Alice Wallenberg Foundation (KAW 2017.0061) and the Swedish Research Council (Vetenskapsrådet, VR 2021-04498_3).

[1] P. Schiffer, A. P. Ramirez, W. Bao, and S. W. Cheong, Low Temperature Magnetoresistance and the Magnetic Phase Diagram of $La_{1-x}Ca_xMnO_3$, Phys. Rev. Lett. **75**, 3336 (1995).

[2] A. P. Ramirez, Colossal magnetoresistance, J. Phys.: Condens. Matter **9**, 8171 (1997).

[3] S. Mühlbauer, B. Binz, F. Jonietz, C. Pfleiderer, A. Rosch, A. Neubauer, R. Georgii, and P. Böni, Skyrmion lattice in a chiral magnet, Science **323**, 915 (2009).

[4] X. Z. Yu, Y. Onose, N. Kanazawa, J. H. Park, J. H. Han, Y. Matsui, N. Nagaosa, and Y. Tokura, Real-space observation of a two-dimensional skyrmion crystal, Nature (London) **465**, 901 (2010).

[5] S. Seki, X. Z. Yu, S. Ishiwata, and Y. Tokura, Observation of skyrmions in a multiferroic material, Science **336**, 198 (2012).

[6] H. Y. Yuan, O. Gomonay, and M. Kläui, Skyrmions and multisublattice helical states in a frustrated chiral magnet, Phys. Rev. B **96**, 134415 (2017).

[7] L. Balents, Spin liquids in frustrated magnets, Nature (London) **464**, 199 (2010).

[8] W. Schweika, M. Valldor, J. D. Reim, and U. K. Rößler, Chiral Spin Liquid Ground State in $YBaCo_3FeO_7$, Phys. Rev. X **12**, 021029 (2022).

[9] A. Oosawa, M. Fujisawa, T. Osakabe, K. Kakurai, and H. Tanaka, Neutron diffraction study of the pressure-induced magnetic ordering in the spin gap system $TlCuCl_3$, J. Phys. Soc. Jpn. **72**, 1026 (2003).

[10] Y. Fujishiro, N. Kanazawa, T. Nakajima, X. Z. Yu, K. Ohishi, Y. Kawamura, K. Kakurai, T. Arima, H. Mitamura, A. Miyake *et al.*, Topological transitions among skyrmion- and hedgehog-lattice states in cubic chiral magnets, Nat. Commun. **10**, 1059 (2019).

[11] T. Suzuki, H. Nagai, M. Nohara, and H. Takagi, Melting of antiferromagnetic ordering in spinel oxide $CoAl_2O_4$, J. Phys.: Condens. Matter **19**, 145265 (2007).

[12] S. B. Lee and L. Balents, Theory of the ordered phase in *a*-site antiferromagnetic spinels, Phys. Rev. B **78**, 144417 (2008).

[13] M. M. Bordelon, C. X. Liu, L. Posthuma, E. Kenney, M. J. Graf, N. P. Butch, A. Banerjee, S. Calder, L. Balents, and S. D. Wilson, Frustrated Heisenberg $J_1 - J_2$ model within the stretched diamond lattice of $LiYbO_2$, Phys. Rev. B **103**, 014420 (2021).

[14] A. P. Ramirez, Geometric frustration: magic moments, Nature (London) **421**, 483 (2003).

[15] R. Moessner, Magnets with strong geometric frustration, Can. J. Phys. **79**, 1283 (2001).

[16] A. P. Ramirez, Strongly geometrically frustrated magnets, Annu. Rev. Mater. Sci. **24**, 453 (1994).

[17] R. Moessner and J. T. Chalker, Properties of a Classical Spin Liquid: The Heisenberg Pyrochlore Antiferromagnet, Phys. Rev. Lett. **80**, 2929 (1998).

[18] H. C. Jiang, M. Q. Weng, Z. Y. Weng, D. N. Sheng, and L. Balents, Supersolid order of frustrated hard-core bosons in a triangular lattice system, Phys. Rev. B **79**, 020409(R) (2009).

[19] K. Yang, W. J. Xu, D. Lu, Y. X. Zhou, L. Liu, Y. Z. H. Ma, G. Y. Wang, and H. Wu, Magnetic frustration in the cubic double perovskite Ba_2NiIrO_6, Phys. Rev. B **105**, 184413 (2022).

[20] R. J. Baxter and F. Y. Wu, Exact Solution of an Ising Model with Three-Spin Interactions on a Triangular Lattice, Phys. Rev. Lett. **31**, 1294 (1973).

[21] P. Santini, S. Carretta, G. Amoretti, R. Caciuffo, N. Magnani, and G. H. Lander, Multipolar interactions in f-electron systems: the paradigm of actinide dioxides, Rev. Mod. Phys. **81**, 807 (2009).

[22] I. A. Sergienko and E. Dagotto, Role of the Dzyaloshinskii-Moriya interaction in multiferroic perovskites, Phys. Rev. B **73**, 094434 (2006).

[23] J. G. Gay and R. Richter, Spin Anisotropy of Ferromagnetic Films, Phys. Rev. Lett. **56**, 2728 (1986).

[24] M. Matsumoto, C. Yasuda, S. Todo, and H. Takayama, Ground-state phase diagram of quantum Heisenberg antiferromagnets on the anisotropic dimerized square lattice, Phys. Rev. B **65**, 014407 (2001).

[25] K. Foyevtsova, I. Opahle, Y. Z. Zhang, H. O. Jeschke, and R. Valentí, Determination of effective microscopic models for the frustrated antiferromagnets Cs_2CuCl_4 and Cs_2CuBr_4 by density functional methods, Phys. Rev. B **83**, 125126 (2011).

[26] H. O. Jeschke, F. Salvat-Pujol, and R. Valentí, First-principles determination of Heisenberg Hamiltonian parameters for the spin-$\frac{1}{2}$ kagome antiferromagnet $ZnCu_3(OH)_6Cl_2$, Phys. Rev. B **88**, 075106 (2013).

[27] A. I. Liechtenstein, M. I. Katsnelson, V. P. Antropov, and V. A. Gubanov, Local spin density functional approach to the theory of exchange interactions in ferromagnetic metals and alloys, J. Magn. Magn. Mater. **67**, 65 (1987).

[28] E. Manousakis, The spin-$\frac{1}{2}$ Heisenberg antiferromagnet on a square lattice and its application to the cuprous oxides, Rev. Mod. Phys. **63**, 1 (1991).

[29] H. Bethe, Zur Theorie der Metalle, Z. Phys. **71**, 205 (1931).

[30] B. S. Shastry and B. Sutherland, Exact ground state of a quantum mechanical antiferromagnet, Physica B+C **108**, 1069 (1981).

[31] A. Kitaev, Anyons in an exactly solved model and beyond, Ann. Phys. **321**, 2 (2006).

[32] D. P. Arovas and A. Auerbach, Functional integral theories of low-dimensional quantum Heisenberg models, Phys. Rev. B **38**, 316 (1988).

[33] E. Dagotto and A. Moreo, Exact diagonalization study of the frustrated Heisenberg model: a new disordered phase, Phys. Rev. B **39**, 4744 (1989).

[34] E. Dagotto and A. Moreo, Phase Diagram of the Frustrated Spin-$\frac{1}{2}$ Heisenberg Antiferromagnet in 2 Dimensions, Phys. Rev. Lett. **63**, 2148 (1989).

[35] M. Suzuki, S. Miyashita, and A. Kuroda, Monte Carlo simulation of quantum spin systems. I, Prog. Theor. Phys. **58**, 1377 (1977).

[36] J. W. Lyklema, Quantum-Statistical Monte Carlo Method for Heisenberg Spins, Phys. Rev. Lett. **49**, 88 (1982).

[37] M. S. Makivić and H. Q. Ding, Two-dimensional spin-$\frac{1}{2}$ Heisenberg antiferromagnet: a quantum Monte Carlo study, Phys. Rev. B **43**, 3562 (1991).

[38] Z. P. Liu and E. Manousakis, Variational calculations for the square-lattice quantum antiferromagnet, Phys. Rev. B **40**, 11437 (1989).

[39] S. R. White, Density Matrix Formulation for Quantum Renormalization Groups, Phys. Rev. Lett. **69**, 2863 (1992).

[40] S. R. White, Density-matrix algorithms for quantum renormalization groups, Phys. Rev. B **48**, 10345 (1993).

[41] H. C. Jiang, Z. Y. Weng, and D. N. Sheng, Density Matrix Renormalization Group Numerical Study of the Kagome Antiferromagnet, Phys. Rev. Lett. **101**, 117203 (2008).

[42] S. M. Yan, D. A. Huse, and S. R. White, Spin-liquid ground state of the $S = \frac{1}{2}$ kagome Heisenberg antiferromagnet, Science **332**, 1173 (2011).

[43] E. M. Stoudenmire and S. R. White, Studying two-dimensional systems with the density matrix renormalization group, Annu. Rev. Condens. Matter Phys. **3**, 111 (2012).

[44] Y. C. He, M. P. Zaletel, M. Oshikawa, and F. Pollmann, Signatures of Dirac Cones in a DMRG Study of the Kagome Heisenberg Model, Phys. Rev. X **7**, 031020 (2017).

[45] H. B. Callen, Green function theory of ferromagnetism, Phys. Rev. **130**, 890 (1963).

[46] J. Kondo and K. Yamaji, Green's-function formalism of the one-dimensional Heisenberg spin system, Prog. Theor. Phys. **47**, 807 (1972).

[47] D. A. Yablonskiy, Tyablikov approximation in the theory of low-dimensional quantum Heisenberg ferromagnets and antiferromagnets, Phys. Rev. B **44**, 4467 (1991).

[48] I. Junger, D. Ihle, J. Richter, and A. Klumper, Green-function theory of the Heisenberg ferromagnet in a magnetic field, Phys. Rev. B **70**, 104419 (2004).

[49] F. Aryasetiawan and S. Biermann, Generalized Hedin's Equations for Quantum Many-Body Systems with Spin-Dependent Interactions, Phys. Rev. Lett. **100**, 116402 (2008).

[50] F. Aryasetiawan and K. Karlsson, Green's function formalism for calculating spin-wave spectra, Phys. Rev. B **60**, 7419 (1999).

[51] M. Hamedoun, Y. Cherriet, A. Hourmatallah, and N. Benzakour, Quantum Heisenberg model with long-range ferromagnetic interactions: a Green's function approach, Phys. Rev. B **63**, 172402 (2001).

[52] See Supplemental Material at https://link.aps.org/supplemental/10.1103/PhysRevB.106.184417 for the detailed account of the approach.

[53] N. Shannon, B. Schmidt, K. Penc, and P. Thalmeier, Finite temperature properties and frustrated ferromagnetism in a square lattice Heisenberg model, Eur. Phys. J. B **38**, 599 (2004).

[54] I. Dzyaloshinsky, A thermodynamic theory of "weak" ferromagnetism of antiferromagnetics, J. Phys. Chem. Solids **4**, 241 (1958).

[55] T. Moriya, Anisotropic superexchange interaction and weak ferromagnetism, Phys. Rev. **120**, 91 (1960).

[56] J. P. Gauyacq and N. Lorente, A model for individual quantal nano-skyrmions, J. Phys.: Condens. Matter **31**, 335001 (2019).